Electron tomography of late stages of FcRn-mediated antibody transcytosis in neonatal rat small intestine

Mark S. Ladinsky[a], Kathryn E. Huey-Tubman[a,b], and Pamela J. Bjorkman[a,b]
[a]Division of Biology and [b]Howard Hughes Medical Institute, California Institute of Technology, Pasadena, CA 91125

ABSTRACT The neonatal Fc receptor (FcRn) transports maternal immunoglobulin (IgG) across epithelia to confer passive immunity to mammalian young. In newborn rodents, FcRn transcytoses IgG from ingested milk across the intestinal epithelium for release into the bloodstream. We used electron tomography to examine FcRn transport of Nanogold-labeled Fc (Au-Fc) in neonatal rat jejunum, focusing on later aspects of transport by chasing Au-Fc before fixation. We observed pools of Au-Fc in dilated regions of the lateral intercellular space (LIS), likely representing exit sites where Au-Fc accumulates en route to the blood. Before weaning, the jejunum functions primarily in IgG transport and exhibits unusual properties: clathrin-rich regions near/at the basolateral LIS and multivesicular bodies (MVBs) expressing early endosomal markers. To address whether these features are related to IgG transport, we examined LIS and endocytic/transcytotic structures from neonatal and weaned animals. Weaned samples showed less LIS-associated clathrin. MVBs labeled with late endosomal/lysosomal markers were smaller than their neonatal counterparts but contained 10 times more internal compartments. These results are consistent with hypotheses that clathrin-rich basolateral regions in neonatal jejunum are involved in IgG exocytosis and that MVBs function in IgG transport while FcRn is expressed but switch to degradative functions after weaning, when the jejunum does not express FcRn or transport IgG.

Monitoring Editor
Keith E. Mostov
University of California, San Francisco

Received: Feb 7, 2012
Revised: Apr 4, 2012
Accepted: May 1, 2012

INTRODUCTION

Tissue epithelia are composed of polarized cells that serve as barriers to infection and protect against nonspecific transfer of exogenous molecules to the bloodstream and underlying tissues. Proteins can cross epithelial cell barriers by receptor-mediated transcytosis, in which membrane-associated receptors bind ligands from the apical or basolateral surface of the cell and transport them to the opposite surface, where the ligand is released (Tuma and Hubbard, 2003). The neonatal Fc receptor (FcRn) is a transcytotic receptor that transports maternal immunoglobulin G (IgG) from the apical (luminal) side of the epithelium to the basolateral side (Rodewald and Kraehenbuhl, 1984; Simister and Rees, 1985; Ward and Ober, 2009), thereby providing the fetus or newborn with humoral immunity before its immune system is fully functional. Passive acquisition of maternal antibodies by mammalian neonates plays a critical role in protection against infectious agents and autoimmune diseases (Zinkernagel, 2001).

FcRn was first discovered in the proximal small intestine of suckling rats (Jones and Waldmann, 1972). The receptor is expressed at the apical surface of a subset of neonatal epithelial cells in the proximal small intestine, where it specifically binds maternal IgG from ingested milk, transcytoses the IgG across the gut epithelium, and then releases it at the basolateral surface into the extracellular space, from where it enters the bloodstream (Brambell, 1966; Rodewald, 1970, 1973, 1980; Rodewald and Kraehenbuhl, 1984; Jones and Waldmann, 1972; Borthistle *et al.*, 1977). The net pH difference between the apical (pH 6.0–6.5) and basolateral (pH 7.4) sides of intestinal epithelial cells facilitates efficient unidirectional transport of

This article was published online ahead of print in MBoC in Press (http://www.molbiolcell.org/cgi/doi/10.1091/mbc.E12-02-0093) on May 9, 2012.

Address correspondence to: Pamela J. Bjorkman (bjorkman@caltech.edu).

Abbreviations used: Au-Fc, Nanogold-labeled Fc fragment of IgG; ET, electron tomography; FcRn, neonatal Fc receptor; HPF/FSF, high-pressure freezing/freeze substitution fixation; IgG, immunoglobulin G; LIS, lateral intercellular space; MVB, multivesicular body.

© 2012 Ladinsky *et al.* This article is distributed by The American Society for Cell Biology under license from the author(s). Two months after publication it is available to the public under an Attribution–Noncommercial–Share Alike 3.0 Unported Creative Commons License (http://creativecommons.org/licenses/by-nc-sa/3.0).
"ASCB®," "The American Society for Cell Biology®," and "Molecular Biology of the Cell®" are registered trademarks of The American Society of Cell Biology.

IgG, since FcRn binds IgG at pH 6.0–6.5 but shows greatly reduced or no binding at neutral or higher pH (Rodewald and Kraehenbuhl, 1984; Simister and Mostov, 1989; Raghavan *et al.*, 1995).

As milk passes through the neonatal digestive system, maternal IgG is specifically taken up by cells in the proximal small intestine (duodenum and jejunum), and remaining proteins are absorbed and degraded by cells in the distal small intestine (ileum; Rodewald, 1970, 1973, 1980; Jones and Waldmann, 1972). Accordingly, FcRn is expressed in the duodenum and jejunum, but not in the ileum, of the suckling rat (Rodewald, 1973). Early electron microscopy (EM) studies of FcRn-mediated IgG transport in neonatal rat intestines revealed that IgG enters the jejunal cells via coated pits on the apical plasma membrane, is sorted into tubular vesicles within the apical cytoplasm, and is then transferred to vesicles that migrate to the basolateral surface and subsequently release the IgG (Rodewald, 1970, 1973; Abrahamson and Rodewald, 1981). After weaning at 3 wk of age, rat jejunal cells undergo distinct morphological changes and no longer express detectable levels of FcRn or specifically transport IgG (Rodewald, 1973; Berryman and Rodewald, 1995).

Advances in cellular electron tomography (ET) have made it possible to investigate FcRn-mediated transport at higher resolution and in three dimensions. We previously reported the use of ET to investigate FcRn-mediated IgG transport across neonatal rat jejunal epithelial cells (He *et al.*, 2008). ET and subsequent three-dimensional segmentation and analysis allowed us to accurately map early events in the FcRn transcytosis pathway, revealing that gold-labeled IgG Fc (Au-Fc; used as an FcRn ligand) traverses epithelial cells via a complex system of apical coated pits, tubular or structurally irregular vesicles tangled together and sometimes aligned with microtubules, multivesicular bodies (MVBs), and basolateral clathrin-coated vesicles and pits (He *et al.*, 2008). The pathways inferred from these snapshots of dynamic events included unexpected features: transport involving MVBs, which are typically assumed to serve as degradative compartments (Morales *et al.*, 1999; Jiang *et al.*, 2002), and apparent exocytosis through clathrin-coated pits. Clathrin coats on trafficking/exocytic vesicles were generally believed to be shed before membrane fusion (Altstiel and Branton, 1983; Brodsky *et al.*, 2001; Conner and Schmid, 2003). However, we argued that the observed Au-Fc–containing clathrin-coated structures represented vesicles caught during partial uncoating and fusion with the basolateral membrane (He *et al.*, 2008). An alternative interpretation, that clathrin-coated pits containing Au-Fc represented structures that were endocytosing extracellular Au-Fc, is unlikely since FcRn does not bind Fc at the basic pH of the basolateral membrane (Rodewald and Kraehenbuhl, 1984; Raghavan *et al.*, 1995).

In this study we expand on our previous work to examine the later stages of FcRn transport in rat neonatal epithelial cells and to characterize the domains at which Au-Fc exits the epithelium en route to the bloodstream. Furthermore, we investigate whether transport by MVBs and clathrin's apparent involvement in exocytosis are features specific to FcRn-expressing neonatal jejunal cells. Using ET and EM immunolabeling, we compare MVBs in jejunal and ileal cells from both neonatal and weaned rats and examine later points in FcRn-mediated transport of IgG by comparing chased and nonchased samples.

RESULTS

Late events in FcRn trafficking

To identify single FcRn-Fc complexes by ET, we developed a general method for localizing specific ligands for studies of dynamic endocytic events (He *et al.*, 2007; Morphew *et al.*, 2008). This approach uses ligands covalently coupled to 1.4-nm Nanogold clusters, which (unlike colloidal gold) do not inhibit endocytosis or induce misdirection of ligand–receptor complexes (Hainfeld and Powell, 2000; He *et al.*, 2007). We made Nanogold-labeled Fc (Au-Fc) and used it as a ligand for FcRn after demonstrating that FcRn transports Fc and IgG equivalently (Tesar *et al.*, 2006) and that Au-Fc binds FcRn with the expected pH dependence (He *et al.*, 2007). Au-Fc is too small to be localized in cellular tomograms (He *et al.*, 2007), and standard gold-enhancement protocols (Danscher, 1981; Hacker *et al.*, 1988; Scopsi, 1989; Hainfeld and Furuya, 1995) are not compatible with high-pressure freezing/freeze substitution fixation (HPF/FSF), which was required for our studies because HPF immobilizes dynamic activity in milliseconds (McIntosh *et al.*, 2005), as opposed to seconds or minutes for chemical fixation, during which time vesicles moving at 1–2 μm/s (Rice *et al.*, 2009; Jerdeva *et al.*, 2010) could traverse the cell before cross-linking occurred. We therefore developed gold-enlarging techniques for HPF/FSF samples (He *et al.*, 2007; Morphew *et al.*, 2008), allowing us to identify and localize single Au-Fc molecules in tomograms prepared from optimally preserved tissue (He *et al.*, 2008).

Our previous ET investigations of FcRn trafficking were done at steady state; that is, intestinal tissue was taken from neonatal rats that had been fed Au-Fc over a period of several hours and then immediately immobilized by HPF (He *et al.*, 2008). By this method, structural aspects of all phases of Au-Fc transport in FcRn-positive cells, including uptake at the apical surface, transport across the cell, exocytosis from the basolateral surface, and entry into the bloodstream, were observed simultaneously. In the present study, we focused on late events of Au-Fc transport, first verifying that ingested Au-Fc was transcytosed properly and reached the neonate's bloodstream. To confirm this, we used inductively coupled plasma mass spectrometry (ICP-MS) to detect gold in neonatal blood samples. In this method, samples are decomposed to their neutral elements in high-temperature argon plasma and then identified and analyzed based on mass-to-charge ratios (Vanhoe, 1993). To monitor the extent of nonspecific delivery, we examined blood from neonatal rats fed gold-labeled dextran (Au-dextran; a marker of fluid-phase endocytosis), as well as blood from weaned rats fed either Au-Fc or Au-dextran, none of which should be delivered to the blood by receptor-mediated transcytosis. Before the animals were killed, blood was removed from neonatal and weaned rats fed Au-Fc, Au-dextran, or buffer alone. ICP-MS analysis of the rat sera revealed an average concentration of 10.8 ± 3.9 mg/l of ^{197}Au in the blood of Au-Fc–fed neonates, representing ~33% of the total Au-Fc that was ingested (see *Materials and Methods*). The ^{197}Au was not detected in the sera of neonatal pups fed Au-dextran or weaned pups fed Au-Fc or Au-dextran at levels above the background determined for neonatal or weaned buffer-fed pups. These results verified that Au-Fc was specifically transferred across the neonatal intestinal epithelium and reached the neonatal bloodstream in our experiments. EM examination of jejunal tissue from neonatal rats fed Au-Fc or Au-dextran and fixed immediately after they were killed confirmed that Au-Fc was found within a variety of endosomal structures (Figure 1A), whereas Au-dextran was detected only in lysosomes (Supplemental Figure S1), further demonstrating the specificity of the Au-Fc–FcRn pathway.

To visualize later aspects of FcRn trafficking by ET, we applied our previous methods (He *et al.*, 2007, 2008) to intestinal tissue in which Au-Fc had been chased for a short time before HPF/FSF. Neonatal rats were fed Au-Fc as before, and intestinal tissue was isolated from the animals and then incubated in culture medium at physiological temperature for extra time before cryoimmobilization (a short chase of

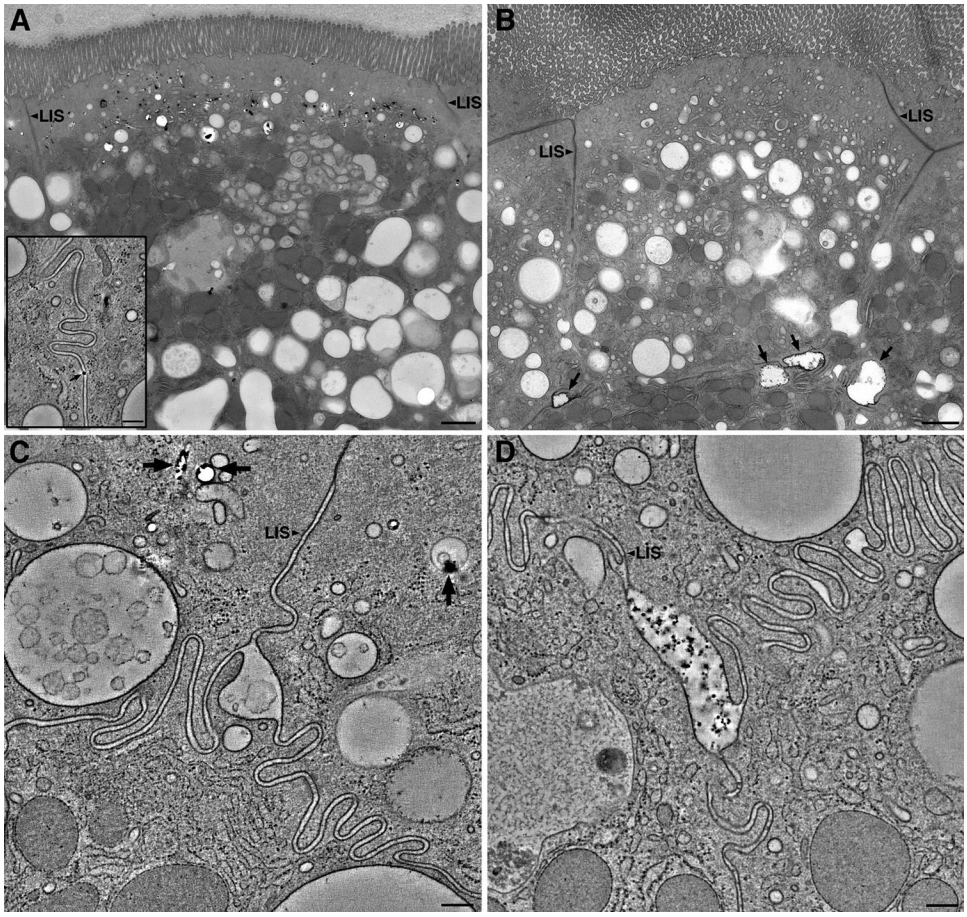

FIGURE 1: Comparison of chased and nonchased neonatal jejunal cells. (A) Overview (projection image) of a nonchased cell, showing Au-Fc in the apical tubular network. Inset, detail of the LIS from a tomographic slice showing a single enhanced Au-Fc (arrow). (B) Overview (projection image) of short-chased (15 min) cell, showing Au-Fc localized to dilated basolateral LIS domains (arrows). (C) Tomographic slice of a dilated LIS domain in a nonchased cell. The dilated LIS region is empty, but Au-Fc is present in nearby endocytic compartments (arrows). (D) Tomographic slice of a dilated LIS domain in a chased cell, showing it is full of Au-Fc. Bars, 1 µm (A, B), 0.2 µm (C, D, inset).

15 min, a medium chase of 30 min, and a long chase of 60 min, as compared with <1 min in nonchased samples). We reasoned that incubating isolated tissue at 37°C would drive the Au-Fc into later stages of its trafficking pathway, possibly allowing it to accumulate at exit points in the epithelial cells without transfer to and subsequent dilution in the bloodstream. The differing chase times were chosen to allow visualization of FcRn-Fc complexes at terminal portions of their transcytotic pathway and were based upon measurements in neonatal rats indicating that ingested IgG takes ~30 min from the time of feeding to be detectable in the blood (Halliday, 1955). After the incubations, tissue samples were cryoimmobilized by HPF, taken through the gold enhancement protocol, embedded, sectioned and analyzed by ET. Intestinal villi were selected at random and tomography was performed on cellular regions that were positive for the enhanced Au-Fc.

Figure 1 compares the localization of enhanced Au-Fc in nonchased neonatal jejunal epithelial cells versus cells that had been chased for a short (15 min) time. Montaged projection images of 200-nm-thick sections display the entirety of each cell in their X-Y dimensions (Figure 1, A and B). Nonchased cells (Figure 1A) show Au-Fc localized to the complex network of tubules and vesicles in the apical cytoplasm, with occasional isolated Au-Fc observed in the LIS (Figure 1A, inset), similar to localizations characterized in our previous work (He *et al.*, 2007, 2008). Cells from short-chased (15 min) samples (Figure 1B) showed Au-Fc in some basolateral vesicles and MVBs, but Au-Fc was found primarily as pools within dilated regions of the lateral intercellular space (LIS), typically at junctions of three or more adjacent cells. Within a given villus, ~30% of dilated LIS regions contained pools of Au-Fc, which were usually evenly filled (Figure 1D). However, sometimes the gold within a dilated region appeared to be concentrated near the walls of the LIS, possibly a result of fluid dynamics or eddies as liquid moved through the channels (Figure 2B). Serial-section tomographic reconstructions revealed that the dilated regions were large, occupying ≥1 µm of reconstructed cellular volume (Figure 2). Dilated LIS regions of similar dimensions were present in nonchased samples (Figure 1C), but these regions were negative for enhanced Au-Fc. The medium-chased (30 min) samples showed very little enhanced gold, but what was detectable was localized to a small number of basolateral compartments rather than to dilated regions of the LIS (Supplemental Figure S2A). Enhanced gold was undetectable in the long-chased (60 min) samples (Supplemental Figure S2B). Taken together, these data suggest that the dilated regions of the LIS containing Au-Fc pools observed in the short-chased samples represent exit sites from the epithelium or domains near exit sites where Au-Fc accumulated en route to the bloodstream.

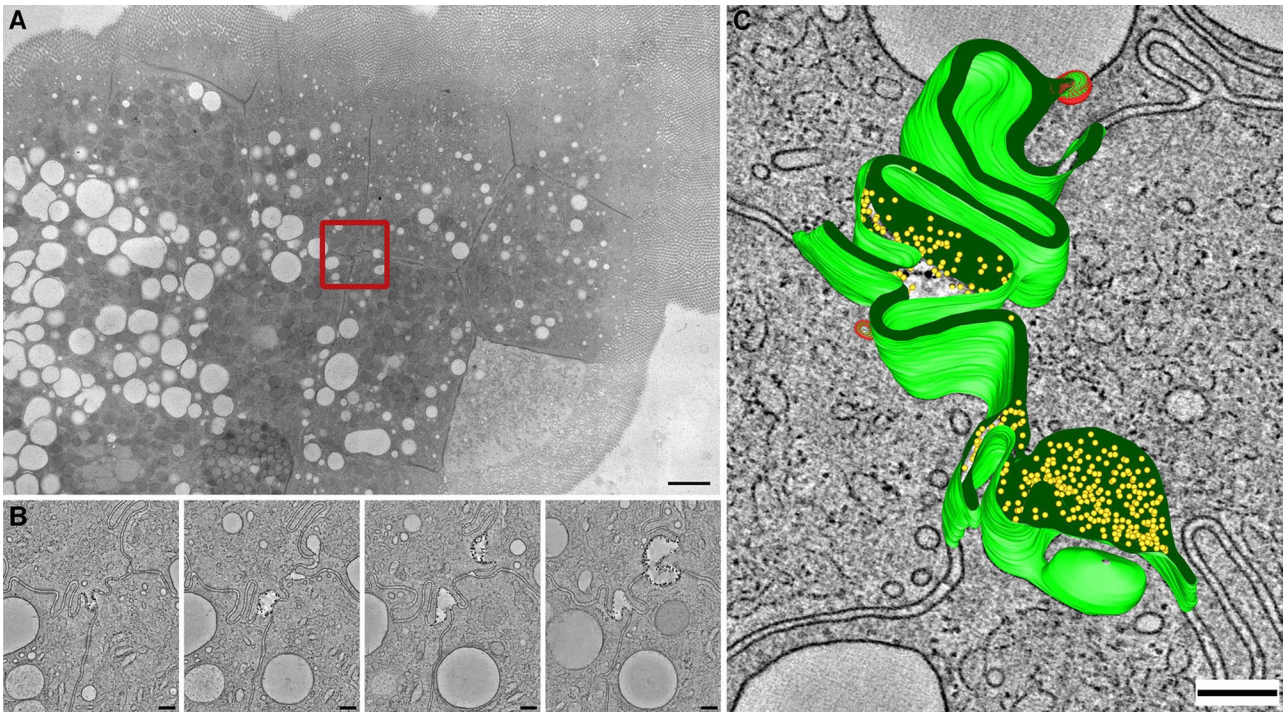

FIGURE 2: Au-Fc–filled LIS domain from a short-chased (15 min) neonatal jejunal cell. (A) Overview of a villus from the neonatal jejunum. The red square indicates a region ($2.8 \times 2.6 \times 0.8$ μm) selected for serial ET. (B) Tomographic slices from each of four serial 200-nm sections. (C) Segmented model of the reconstructed region superimposed over a single tomographic slice. Green, LIS membranes; gold spheres, enhanced Au-Fc; red stippling, clathrin-coated buds. Bars, 2 μm (A), 0.2 μm (B, C).

Comparison of basolateral LIS in jejunum and ileum before and after weaning

The neonatal small intestine functions almost exclusively in transport of IgG to the bloodstream (Rodewald, 1973). Before weaning, protein uptake by jejunal cells is restricted primarily to IgG, whereas other milk and serum proteins are taken up by ileal cells, where they are digested rather than transferred to the blood (Jones and Waldmann, 1972; Rodewald, 1973). Consistent with their different functions, epithelial cells in the proximal and distal small intestine differ in appearance (Rodewald, 1973). Neonatal jejunal epithelial cells are characterized by a complex network of endocytic tubules and vesicles located primarily in the apical cytoplasm (Figure 3A). In contrast, neonatal ileal cells contain a large supranuclear vacuole or giant lysosome, and their apical cytoplasm contains smaller vacuoles and an interconnected system of vesicles (Figure 3B). These vesicles display a distinct "beaded" membrane structure composed of regularly spaced particles (Rodewald, 1973; Knutton *et al.*, 1974; Fujita *et al.*, 1990). After weaning, jejunal epithelial cells lose the apical tubular array, and the region that it previously occupied contains rough endoplasmic reticulum, mitochondria, and other organelles, similar to typical epithelial cells (Figure 3C). Epithelial cells of the ileum undergo equally dramatic changes at weaning, with the loss of both the giant lysosomes and the apical tubular network (Figure 3D).

In our previous study of the neonatal jejunum (He *et al.*, 2008), we noted unusually large numbers of clathrin-coated vesicles in the vicinity of the basolateral LIS near the tight junctions (i.e., apical to the regions shown in Figures 1, C and D, and 2, B and C) and speculated that they were involved in exocytosis of Au-Fc (see Figure 5, B–G, and Supplemental Movies S6 and S7 in He *et al.*, 2008). To determine whether this feature was exclusively found in proximal small intestinal cells during the time period when FcRn mediates IgG transport (before weaning), we compared regions of the basolateral LIS in samples of jejunum and ileum from both neonatal and weaned animals (Figure 4). Similar to our previous work, abundant clathrin was found in association with the LIS in neonatal jejunum (Figure 4A). Less was seen in weaned jejunum (Figure 4B), where most clathrin was associated with *trans*-Golgi (Figure 4B, inset) or coated pits at the plasma membranes. The LIS of neonatal ileum, which was conspicuously straighter and less convoluted than that of the other samples (Figure 4C), was devoid of clathrin, as was the LIS of weaned ileum (Figure 4D).

Structural and functional changes in MVBs after weaning

We previously described an unexpected observation in neonatal jejunal cells, in which it appeared that MVBs play a role in transporting IgG as part of the FcRn-Fc transcytotic pathway (He *et al.*, 2008), contrary to their typically assumed degradative function (Morales *et al.*, 1999; Jiang *et al.*, 2002). Consistent with this hypothesis, we demonstrated that neonatal jejunal MVBs exhibited hallmarks of early, rather than late, endosomes: they contained relatively few internal vesicles (Mari *et al.*, 2008; van Meel and Klumperman, 2008) and labeled with markers for early and recycling endosomes (Rab 5 and Rab 11, respectively) but not late endosomes (Rab 7 and Rab 9; He *et al.*, 2008).

To determine whether these unusual features of MVBs were restricted to FcRn-expressing neonatal jejunal cells, we used ET to compare MVBs in jejunal and ileal cells from both neonatal and weaned animals (Figure 5). Using a classification method established for MVBs in human hepatoma cells, in which MVBs with one to eight internal compartments were considered early endosomes and those with nine or more internal compartments were designated as late

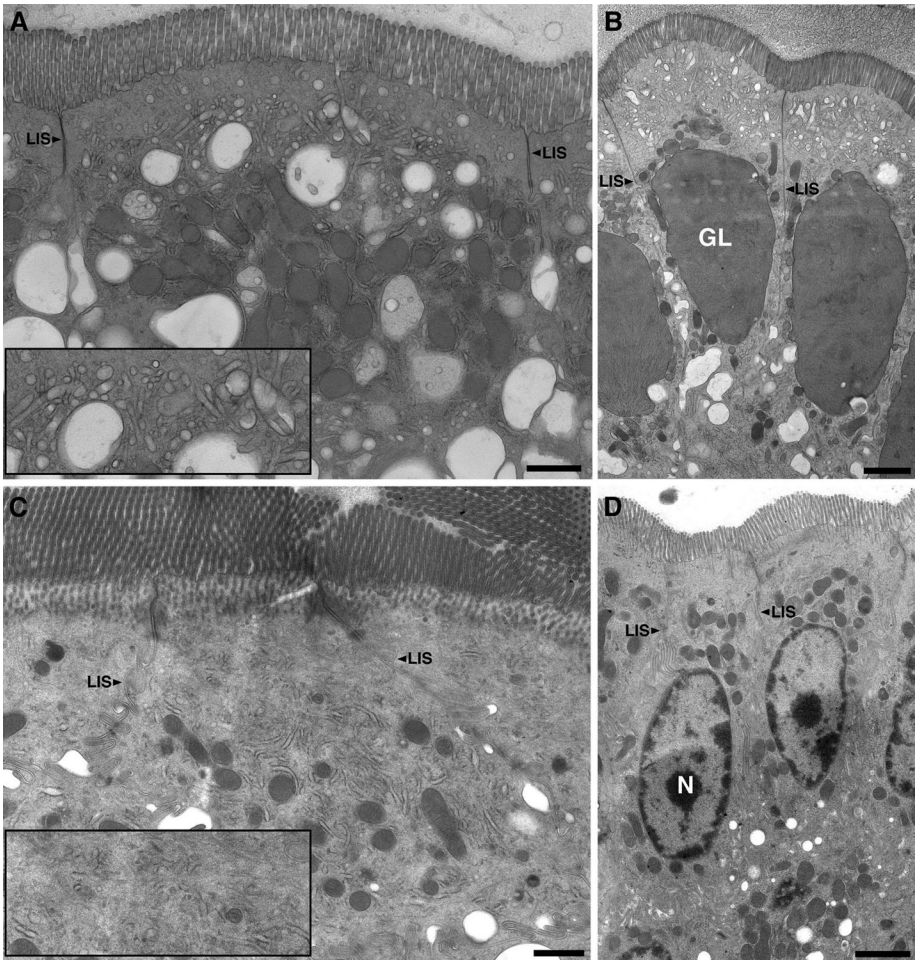

FIGURE 3: Overview comparison of jejunal and ileal cells from neonatal and weaned animals. (A) Neonatal jejunal epithelial cell. Inset, detail of the apical tubular network. (B) Neonatal ileum, showing apical tubular network and the giant lysosome (GL). (C) Weaned jejunal epithelial cell. Inset shows the lack of a tubular network in the apical cytoplasm. (D) Weaned ileum, showing the lack of a tubular network and the nucleus (N) in the place previously occupied by the giant lysosome. Bars, 1 µm (A, C), 2 µm (B, D).

endosomes (Mari *et al.*, 2008; van Meel and Klumperman, 2008), we found the majority of MVBs in both neonatal jejunum and ileum could be classified as early endosomes, whereas MVBs in weaned cells from both locations were classified as late endosomes. For example, the average number of internal compartments in neonatal samples was four in the jejunum and six in the ileum, as compared with 46 and 86, respectively, in their weaned counterparts. Despite the larger number of internal compartments in weaned samples, the outer diameters of MVBs were larger in neonatal samples than in the weaned samples; on average, neonatal jejunal and ileal MVBs were 434 and 548 nm, respectively, while those in weaned samples were 297 and 417 nm, respectively.

To further characterize the potential transport functions of neonatal MVBs, we conducted immunolabeling studies using markers for early endosomes (Rab5) and lysosomes (LAMP1). We found that MVBs from weaned jejunal samples were Rab5 negative but LAMP1 positive, similar to MVBs from the weaned ileum, which showed the same labeling patterns (Figure 6). By contrast, neonatal ileal MVBs shared characteristics with neonatal jejunal MVBs (He *et al.*, 2008) by labeling with Rab5 but not LAMP1.

DISCUSSION

The small intestine of the neonatal rodent serves two major roles: FcRn-mediated transfer of maternal IgG in proximal cells (duodenum and jejunum) and non–receptor-mediated (fluid-phase) uptake and intracellular

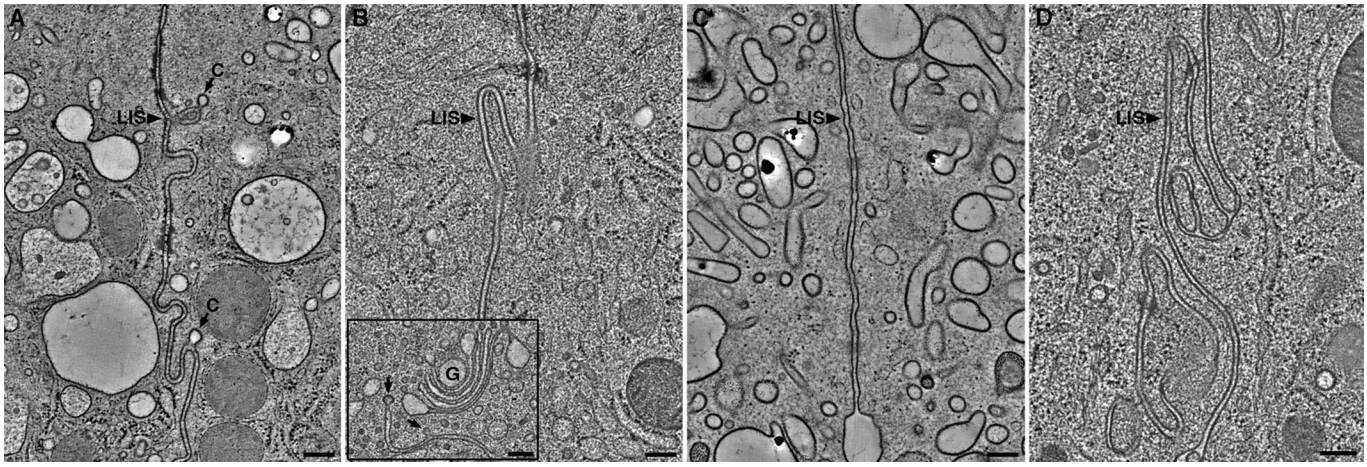

FIGURE 4: Comparison of LIS regions in jejunal and ileal cells from neonatal and weaned animals. (A) Neonatal jejunum (C, clathrin-coated buds within the LIS). (B) Weaned jejunum. Clathrin-coated buds were not found at the LIS. The only clathrin observed was associated with the *trans*-Golgi (inset) or coated pits at the apical plasma membranes. (C) Neonatal ileum. The LIS was devoid of clathrin and conspicuously straighter than in other segments. (D) Weaned ileum; the LIS also lacked clathrin. Bars, 0.2 µm.

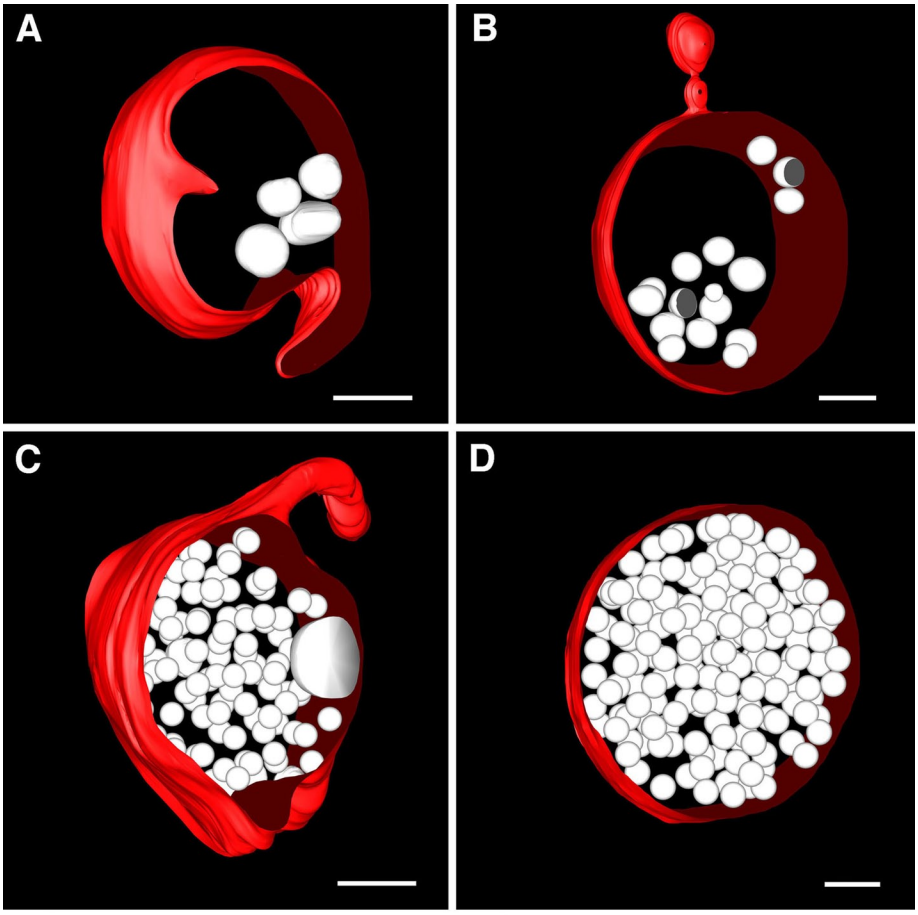

E

MVB Location	n	Average # Internal Compartments	Range	Average Outer Diameter
Neonatal Jejunum	26	4	1 - 15	434 nm
Neonatal Ileum	6	6	1 - 17	548 nm
Weaned Jejunum	14	46	16 - 108	297 nm
Weaned Ileum	10	86	21 - 178	417 nm

FIGURE 5: Properties of MVBs in epithelial cells from the proximal and distal small intestine of neonatal and weaned rats. Segmented three-dimensional models of representative MVBs from tomograms of neonatal jejunum (A), neonatal ileum (B), weaned jejunum (C), weaned ileum (D). Bars, 0.1 μm. (E) Summary of MVB properties (n, number of MVBs in each sample; range, lowest to highest number of internal compartments per MVB).

digestion of proteins for nutrition in distal cells (ileum). Transcytosis in the duodenum and jejunum is highly specific for IgG, whereas other milk and serum proteins are absorbed and digested primarily by ileal cells (Rodewald, 1970, 1973, 1980; Jones and Waldmann, 1972). Transfer of IgG to the blood via the duodenum and jejunum is efficient, whereas proteins endocytosed by ileal cells are transferred into the blood inefficiently or not at all (Jones and Waldmann, 1972; Rodewald, 1973). Here we used ET to examine transport of ingested Au-Fc (serving as a marker for maternal IgG) across neonatal rat intestinal cells, focusing on later events in the transcytotic pathway and morphological differences in the cells as a function of their location in the small intestine and age of the newborn rodent. We first verified the presence of ingested Au-Fc in the neonate's blood using ICP-MS, thus validating that Au-Fc serves as a functional surrogate for maternal IgG and is properly transferred into the bloodstream.

Because traditional pulse-chase methods are not possible with an ingested ligand, since it would be difficult to synchronize uptake in a live animal, we investigated late events in FcRn-mediated transport by incubating jejunal tissue excised from Au-Fc–fed neonatal rats in culture medium at 37°C to chase ingested Au-Fc through the epithelial cells. Similar to our previous studies, which were conducted at steady state (He *et al.*, 2008), we found Au-Fc in basolaterally oriented vesicles and MVBs, but we also observed large pools of enhanced Au-Fc within dilated regions of the LIS, usually at junctions of three adjacent cells. We speculate that these pools represent domains at or near sites where Au-Fc exits from cells en route to the bloodstream, which we were able to visualize because factors required to move IgG away from epithelial exit domains and into the bloodstream were disrupted upon removal of tissue from the animal. This chase methodology enabled us to visualize Au-Fc after it had exited from cells but before it entered the blood, demonstrating a late time point in FcRn-mediated IgG transport. In the steady-state samples that were not chased, we assume that Au-Fc did not accumulate because, while still in the animal, it was able to progress normally into the bloodstream, where it was subsequently diluted.

We also used ET and immuno-EM to further investigate two unexpected features of FcRn-expressing neonatal jejunal cells that we had noted in our previous work (He *et al.*, 2008): large amounts of clathrin at and near the basolateral LIS and MVBs with characteristics similar to early endosomes rather than degradative compartments. First, consistent with its proposed role in Au-Fc exocytosis (He *et al.*, 2008), we found accumulations of clathrin-coated structures near the basolateral LIS only in neonatal jejunal cells, which express FcRn and transport IgG, but not in weaned jejunal cells or in ileal cells from either neonatal or weaned rodents, none of which express FcRn or transport IgG (Rodewald, 1973; Beryman and Rodewald, 1995). Second, MVBs that were structurally and functionally similar to early endosomes in that they contained small numbers of internal compartments and labeled positively for early endosomal markers (Mari *et al.*, 2008; van Meel and Klumperman, 2008) were found exclusively in neonatal cells, not in the epithelial cells of weaned jejunum and ileum, where MVBs contained large numbers of internal compartments and labeled with lysosomal markers, as expected for traditional degradative compartments. These results support the hypothesis that MVBs in the neonatal small intestine serve a role other than their typically assumed degradative function (Morales *et al.*, 1999; Jiang *et al.*, 2002). We propose that neonatal jejunal MVBs are involved in FcRn-mediated transport of IgG (He *et al.*, 2008), analogous to the trafficking of major histocompatibility complex –peptide complexes by MVBs in dendritic

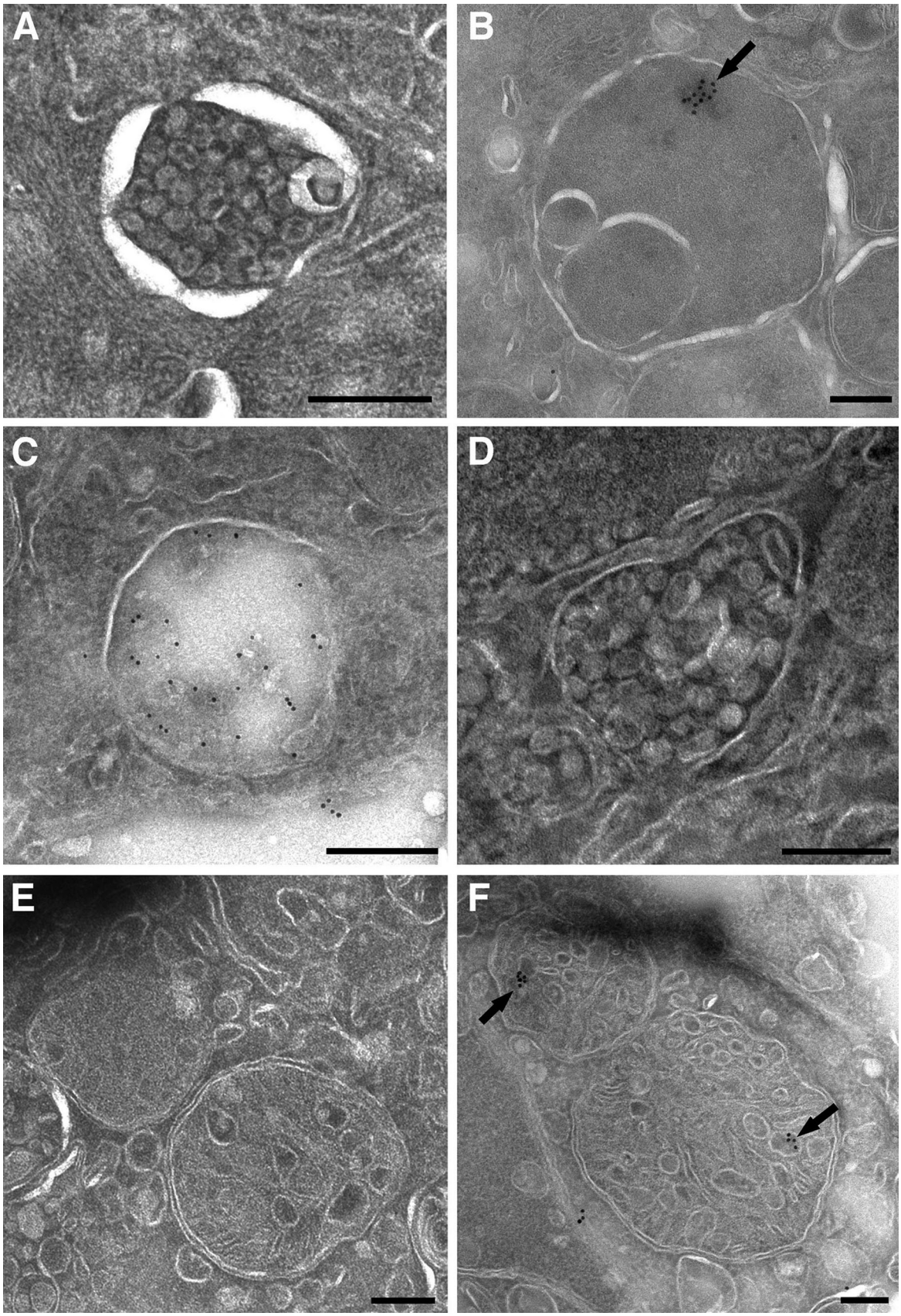

FIGURE 6: Immunolocalization of early endosomal (Rab5) and lysosomal (LAMP1) markers in MVBs of weaned jejunum and neonatal and weaned ileum. Weaned jejunum MVBs were negative for Rab5 (A) but positive for LAMP1 (B, arrow). Neonatal ileum MVBs were positive for Rab5 (C) but negative for LAMP1 (D). Weaned ileum MVBs were negative for Rab5 (E) but positive for LAMP1 (F, arrows). Bars, 0.2 µm.

cells (Kleijmeer *et al.*, 2001). Consistent with this hypothesis, we found that Au-Fc in jejunal MVBs was associated specifically with the inner leaflet of the main MVB membrane, the outsides of inner vesicles, and the inside of tubular protrusions, suggesting that Fc within MVBs remained bound to FcRn (He *et al.*, 2008). By contrast, Au-Fc was randomly distributed in ileal compartments, where IgG and other proteins are degraded (Jones and Waldmann, 1972; He *et al.*, 2008). Similar to the neonatal jejunum, MVBs in the neonatal ileum may serve a transport role as well, as we observed that they also contained small numbers of internal compartments and expressed markers of early endosomes. This suggests that the giant lysosomes, which disappear from ileal cells after weaning, serve as an exclusive or near-exclusive site for degradation of nutrients from milk. Taken together, these studies reveal unusual properties of the neonatal intestine during the time that it is specialized for absorbing IgG and nutrients from milk.

MATERIALS AND METHODS

Preparation of Au-Fc and Au-dextran

Wild-type rat Fc was expressed, purified, and labeled with 1.4-nm monomaleimido Nanogold (Nanoprobes, Yaphank, NY) as described (He *et al.*, 2007). Au-Fc was purified by both gel filtration and FcRn affinity chromatography, ensuring that Au-Fc did not contain aggregates and that it retained pH-dependent binding to FcRn (He *et al.*, 2007). Sulfo-NHS Nanogold (Nanoprobes) was attached to primary amines on dextran as described (He *et al.*, 2007), and labeled molecules were purified by gel filtration chromatography.

Ligand uptake and ICP-MS

Experiments were performed on neonatal (10–13 d old) or weaned (21–25 d old) rat pups as previously described (He *et al.*, 2008). Briefly, rat pups were fasted for 3 h, dosed three times at 45-min intervals with 100 µl of 3 µM Au-Fc, 3 µM Au-dextran, or buffer, which they drank freely from a gavage needle. Pups were anesthetized after 1.5 h, and blood samples for ICP-MS analyses were collected by cardiac puncture prior to the pups being killed and tissue collection. Blood samples were incubated at room temperature for 1 h to allow clotting, after which sera were harvested by centrifugation at 2000 × *g* for 15 min. Serum samples were stored at −80°C before digestion and analysis. Thawed sera were digested with 68% Aristar Ultra nitric acid (trace metal analysis grade) at 70°C and then diluted with 2% nitric acid for ICP-MS analysis. Digested and diluted serum samples were analyzed using an X-Series II ICP-MS (Thermo Scientific, West Palm Beach, FL). For calculating gold concentrations, standard dilution series (0–100 µg/l) were generated by diluting a gold standard (EMD, Rockland, MA), monomaleimido Nanogold, or Au-Fc in 2% nitric acid, or by spiking serum samples with 30 mg/l of the EMD gold standard, monomaleimido Nanogold, or purified Au-Fc (digested and analyzed as described), and ^{197}Au counts were averaged from three serum samples. Samples spiked with Au-Fc routinely resulted in ^{197}Au counts that were ~10% of the values for gold standards not coupled to Fc, and thus the concentrations calculated from the standard curves included a correction factor to account for lower counts for Fc-coupled gold. The ^{197}Au counts for sera from Au-dextran–fed neonatal pups and Au-Fc– or Au-dextran–fed weaned pups were not significantly different from ^{197}Au counts in buffer-fed neonatal or weaned pups, and thus only background levels of ^{197}Au were detected in these samples. The only serum samples containing ^{197}Au counts above background were in the three samples from Au-Fc–fed neonatal pups. These samples contained an average of 10.8 mg/l Au-Fc, representing ~33% of the total Au-Fc (0.9 nmol) fed to a neonatal pup diluted into its 1.5-ml blood volume.

Tissue preparation for EM

After the animals were killed, samples were prepared by removing tissue from Au-Fc–fed, Au-dextran–fed, or buffer-fed animals and cryopreserving by HPF. For nonchased samples, tissue was excised from the animal and high-pressure frozen within 1 min as described (He *et al.*, 2007, 2008). For chased samples, excised tissue was placed in dishes containing Eagle's minimum essential medium, pH 7.2 (Cellgro, Manassas, VA), supplemented with 10% bovine serum and incubated at 37°C with 5% CO_2 for 15, 30, or 60 min before HPF.

High-pressure freezing and freeze substitution fixation

Tissue was quickly trimmed to ~1-mm^3 pieces and transferred to aluminum or brass planchettes (Ted Pella, Redding, CA) that were prefilled with serum-free medium containing 10% Ficoll as an extracellular cryoprotectant. The planchettes were then closed and rapidly frozen in a Bal-Tec HPM-010 high-pressure freezer (Leica Microsystems, Vienna, Austria) and immediately transferred to liquid nitrogen for storage. Low-temperature gold enhancement and FSF were performed as previously described (He *et al.*, 2007, 2008), using an AFS freeze-substitution machine (Leica Microsystems). After low-temperature processing, samples were warmed to room temperature, infiltrated into Epon-Araldite resin (Electron Microscopy Sciences, Port Washington, PA), and flat embedded between a pair of Teflon-coated glass slides. Resin was polymerized at 60°C for 48 h.

Electron microscopy and tomography

Regions of embedded intestinal tissue were selected using a phase-contrast light microscope (Diaphot-200; Nikon, Melville, NY), and then excised and remounted onto plastic sectioning stubs with epoxy glue. Semithick (200 nm) serial sections were cut with an EM-UC6 ultramicrotome (Leica Microsystems) using a diamond knife (Diatome, Biel, Switzerland). Ribbons of sections were transferred to Formvar-coated, 1-mm-slot grids and stained with 3% aqueous uranyl acetate and Reynold's lead citrate. Colloidal gold particles (10 nm) were placed on both surfaces of the grid to serve as fiducial markers for subsequent image alignment. Grids were placed in a Model 2040 dual-axis tomography holder (Fischione Instruments, Export, PA) and imaged in a Tecnai-12 G2 transmission electron microscope (FEI, Hillsboro, OR) operating at 120 KeV. Dual-axis tilt series were acquired automatically using the SerialEM software package (Mastronarde, 2005), with images taken at 1° increments over ±60° about orthogonal axes. Tomograms were calculated, analyzed, and segmented using the IMOD software package (Kremer *et al.*, 1996; Mastronarde, 1997) on a MacPro computer (Apple, Cupertino CA). For display, 10 tomographic slices were joined to represent 15.7 nm of sample thickness. For three-dimensional models, contours were traced and segmented in each 1.5-nm tomographic slice in which an object of interest was present.

Immuno–electron microscopy

Immuno-EM was performed as previously described (He *et al.*, 2008). Briefly, tissue was excised and fixed with 8% paraformaldehyde (Electron Microscopy Sciences, Hatfield, PA) in phosphate-buffered saline (PBS) with 5% sucrose and 0.1 M 4-(2-hydroxyethyl)-1-piperazineethanesulfonic acid on ice for 2–4 h. Samples were then cut to 0.5- to 1-mm^3 blocks and infiltrated with 2.1 M sucrose in PBS over 8–10 h. Blocks were mounted onto aluminum sectioning stubs and quickly frozen in liquid nitrogen. Thin (90 nm) cryosections were cut at −110°C with an EM-UC6/FC6 cryoultramicrotome using a 35° Cryo-Immuno diamond knife (Diatome). Sections

were picked up in a drop of 2.3 M sucrose in PBS with a loop and transferred to Formvar-coated, carbon-coated, glow-discharged 100-mesh EM grids and floated on a pool of PBS. Nonspecific antibody-binding sites were blocked by incubating the sections with 10% calf serum in PBS for 30 min and then labeled with primary and gold-conjugated secondary antibodies, diluted in 5% serum in PBS. Rabbit polyclonal anti-Rab5 (SC-28570) and goat polyclonal anti-LAMP1 (SC-34245) antibodies were purchased from Santa Cruz Biotechnology (Santa Cruz, CA). Colloidal gold conjugated anti-rabbit and anti-goat antibodies were purchased from Ted Pella. Labeled sections were negatively stained with 1% uranyl acetate and stabilized with methylcellulose. Grids were viewed in a Tecnai T12 G2 transmission electron microscope and images recorded digitally.

ACKNOWLEDGMENTS

We thank Grant Jensen and his laboratory for use of the transmission electron microscope and Nathan F. Dalleska and the Caltech Environmental Analysis Center (Pasadena, CA) for assistance with ICP-MS. This work was supported by the National Institutes of Health (2 R37 AI041239-06A1 to P.J.B.) and gifts from the Gordon and Betty Moore Foundation and the Agouron Institute to support electron microscopy at Caltech.

REFERENCES

Abrahamson DR, Rodewald R (1981). Evidence for the sorting of endocytic vesicle contents during the receptor-mediated transport of IgG across the newborn rat intestine. J Cell Biol 91, 270–280.

Altstiel L, Branton D (1983). Fusion of coated vesicles with lysosomes: measurement with a fluorescence assay. Cell 32, 921–929.

Berryman M, Rodewald R (1995). β2-Microglobulin co-distributes with the heavy chain of the intestinal IgG Fc receptor throughout the transepithelial transport pathway of the neonatal rat. J Cell Sci 108, 2347–2360.

Borthistle BK, Kubo RT, Brown WR, Grey HM (1977). Studies on receptors for IgG on epithelial cells of the rat intestine. J Immunol 119, 471–476.

Brambell FW (1966). The transmission of immunity from mother to young and the catabolism of immunoglobulins. Lancet 2, 1087–1093.

Brodsky FM, Chen CY, Knuehl C, Towler MC, Wakeham DE (2001). Biological basket weaving: formation and function of clathrin-coated vesicles. Annu Rev Cell Dev Biol 17, 517–568.

Conner SD, Schmid SL (2003). Regulated portals of entry into the cell. Nature 422, 37–44.

Danscher G (1981). Histochemical demonstration of heavy metals. A revised version of the sulphide silver method suitable for both light and electronmicroscopy. Histochemistry 71, 1–16.

Fujita M, Reinhart F, Neutra M (1990). Convergence of apical and basolateral endocytic pathways at apical late endosomes in absorptive cells of suckling rat ileum in vivo. J Cell Sci 97, 385–394.

Hacker GW, Grimelius L, Danscher G, Bernatzky G, Muss W, Adam H, Thurner J (1988). Silver acetate autometallography—an alternative enhancement technique for immunogold-silver staining (IGSS) and silver amplification of gold, silver, mercury and zinc in tissues. J Histotechnol 11, 213–221.

Hainfeld JF, Furuya FR (1995). Silver-enhancement of Nanogold and undecagold. Immunogold-Silver Staining: Principles, Methods and Applications, ed. MA Hayat, Boca Raton, FL: CRC Press, 71–96.

Hainfeld JF, Powell RD (2000). New frontiers in gold labeling. J Histochem Cytochem 48, 471–480.

Halliday R (1955). The absorption of antibodies from immune sera by the gut of the young rat. Proc R Soc Lond B Biol Sci 143, 408–413.

He W, Kivork C, Machinani S, Morphew MK, Gail AM, Tesar DB, Tiangco NE, McIntosh JR, Bjorkman PJ (2007). A freeze substitution fixation-based gold enlarging technique for EM studies of endocytosed Nanogold-labeled molecules. J Struct Biol 160, 103–113.

He W, Ladinsky MS, Huey-Tubman KE, Jensen GJ, McIntosh JR, Bjorkman PJ (2008). FcRn-mediated antibody transport across epithelial cells revealed by electron tomography. Nature 455, 542–546.

Jerdeva GV, Tesar DB, Huey-Tubman KE, Ladinsky MS, Fraser SE, Bjorkman PJ (2010). Comparison of FcRn- and pIgR-mediated transport in MDCK cells by fluorescence confocal microscopy. Traffic 11, 1205–1220.

Jiang L, Erickson A, Rogers J (2002). Multivesicular bodies: a mechanism to package lytic and storage functions in one organelle? Trends Cell Biol 12, 362–367.

Jones EA, Waldmann TA (1972). The mechanism of intestinal uptake and transcellular transport of IgG in the neonatal rat. J Clin Invest 51, 2916.

Kleijmeer M *et al*. (2001). Reorganization of multivesicular bodies regulates MHC class II antigen presentation by dendritic cells. J Cell Biol 155, 53–63.

Knutton S, Limbrick AR, Robertson JD (1974). Regular structures in membranes. I. Membranes in the endocytic complex of ileal epithelial cells. J Cell Biol 62, 679–694.

Kremer JR, Mastronarde DN, McIntosh JR (1996). Computer visualization of three-dimensional image data using IMOD. J Struct Biol 116, 71–76.

Mari M, Bujny MV, Zeuschner D, Geerts WJ, Griffith J, Petersen CM, Cullen PJ, Klumperman J, Geuze HJ (2008). SNX1 defines an early endosomal recycling exit for sortilin and mannose 6-phosphate receptors. Traffic 9, 380–393.

Mastronarde DN (1997). Dual-axis tomography: an approach with alignment methods that preserve resolution. J Struct Biol 120, 343–352.

Mastronarde DN (2005). Automated electron microscope tomography using robust prediction of specimen movements. J Struct Biol 152, 36–51.

McIntosh JR, Nicastro D, Mastronarde DN (2005). New views of cells in 3D: an introduction to electron tomography. Trends Cell Biol 15, 43–51.

Morales CR, Zhao Q, Lefrancois S (1999). Biogenesis of lysosomes by endocytic flow of plasma membrane. Biocell 23, 149–160.

Morphew M, He W, Bjorkman PJ, McIntosh JR (2008). Silver enhancement of Nanogold particles during freeze substitution for electron microscopy. J Microsc 230, 263–267.

Raghavan M, Bonagura VR, Morrison SL, Bjorkman PJ (1995). Analysis of the pH dependence of the neonatal Fc receptor/Immunoglobulin G interaction using antibody and receptor variants. Biochemistry 34, 14649–14657.

Rice AE, Mendez MJ, Hokanson CA, Rees DC, Bjorkman PJ (2009). Investigation of the biophysical and cell biological properties of ferroportin, a multipass integral membrane protein iron exporter. J Mol Biol 386, 717–732.

Rodewald R (1970). Selective antibody transport in the proximal small intestine of the neonatal rat. J Cell Biol 45, 635–9193.

Rodewald R (1973). Intestinal transport of antibodies in the newborn rat. J Cell Biol 58, 189–211.

Rodewald R (1980). Distribution of immunoglobulin G receptors in the small intestine of the young rat. J Cell Biol 85, 18–32.

Rodewald R, Kraehenbuhl J-P (1984). Receptor-mediated transport of IgG. J Cell Biol 99, S159–S164.

Scopsi L (1989). Silver-enhanced colloidal gold method. Colloidal Gold: Principles, Methods, Applications, ed. MA Hayat, San Diego, CA: Academic Press, 252–288.

Simister NE, Mostov KE (1989). An Fc receptor structurally related to MHC class I antigens. Nature 337, 184–187.

Simister NE, Rees AR (1985). Isolation and characterization of an Fc receptor from neonatal rat small intestine. Eur J Immunol 15, 733–738.

Tesar DB, Tiangco NE, Bjorkman PJ (2006). Ligand valency affects transcytosis, recycling and intracellular trafficking mediated by the neonatal Fc receptor. Traffic 7, 1127–1142.

Tuma PL, Hubbard AL (2003). Transcytosis: crossing cellular barriers. Physiol Rev 83, 871–932.

van Meel E, Klumperman J (2008). Imaging and imagination: understanding the endo-lysosomal system. Histochem Cell Biol 129, 253–266.

Vanhoe H (1993). A review of the capabilities of ICP-MS for trace element analysis in body fluids and tissues. J Trace Elem Electrolytes Health Dis 7, 131–139.

Ward ES, Ober RJ (2009). Multitasking by exploitation of intracellular transport functions: the many faces of FcRn. Adv Immunol 103, 77–115.

Zinkernagel RM (2001). Maternal antibodies, childhood infections, and autoimmune diseases. N Engl J Med 345, 1331–1335.